

Nonequilibrium dynamics in the $O(N)$ model to next-to-next-to-leading order in the $1/N$ expansion

Gert Aarts*

Department of Physics, University of Wales Swansea, Singleton Park, Swansea, SA2 8PP, United Kingdom

Anders Tranberg†

Department of Physics & Astronomy, University of Sussex, Falmer, Brighton, BN1 9QH, United Kingdom and DAMTP, University of Cambridge, Wilberforce Road, Cambridge, CB3 0WA, United Kingdom

(Received 21 April 2006; published 6 July 2006)

Nonequilibrium dynamics in quantum field theory has been studied extensively using truncations of the 2PI effective action. Both $1/N$ and loop expansions beyond leading order show remarkable improvement when compared to mean-field approximations. However, in truncations used so far, only the leading-order parts of the self-energy responsible for memory loss, damping and equilibration are included, which makes it difficult to discuss convergence systematically. For that reason we derive the real and causal evolution equations for an $O(N)$ model to next-to-next-to-leading order in the 2PI- $1/N$ expansion. Because of the appearance of internal vertices the resulting equations appear intractable for a full-fledged $3 + 1$ dimensional field theory. Instead, we solve the closely related three-loop approximation in the auxiliary-field formalism numerically in $0 + 1$ dimensions (quantum mechanics) and compare to previous approximations and the exact numerical solution of the Schrödinger equation.

DOI: [10.1103/PhysRevD.74.025004](https://doi.org/10.1103/PhysRevD.74.025004)

PACS numbers: 11.15.Pg, 05.70.Ln

I. INTRODUCTION

The two-particle irreducible (2PI) effective action formalism has proven very powerful for out-of-equilibrium quantum field theory over a wide range of applications [1]. Since it necessarily employs an expansion and truncation of the effective action, one should be concerned with how well these expansions converge [2].

An extensive study has been made of effective mean-field approximations [Gaussian, leading order (LO) $1/N$ or Hartree approximations] which amounts to including a self-consistent, time-dependent effective mass in the dynamics of the one- and two-point functions [3]. However, since such an approximation does not include scattering, phenomena such as damping, memory loss and equilibration cannot be described properly. This can be traced back to the existence of (infinitely many) conserved charges in the mean-field dynamics and the presence of a nonthermal fixed point [4–6]. Going beyond the mean-field approximation, by either employing the weak coupling or the $1/N$ expansion to next-to-leading order (NLO), effective memory loss, damping and equilibration are present [7]. In particular, it has been found that at late times the system evolves towards a quantum equilibrium state, characterized by suitably defined field occupation numbers approaching the familiar Bose-Einstein or Fermi-Dirac distribution functions. The self-consistently determined propagators have a time-dependent mass and width. It is found therefore that NLO approximations improve dramatically upon mean-field approximations and qualitatively reproduce the

dynamics expected on physical grounds from the full, untruncated system.

The natural question to ask is whether a truncation at NLO also gives quantitatively correct results. This issue has been investigated in several ways, usually by comparing the NLO results to other available approximations. For example, when the coupling is small, normal perturbation theory should be applicable for e.g. estimates of damping rates. Indeed, the results in Ref. [8] suggest that the perturbative result is reproduced within a factor of 2 for small coupling, where the difference is due to the effect of including self-consistent infinite resummations in the 2PI approach. However, this amounts to a test of perturbation theory rather than a verification of the 2PI formalism. Similarly, it is well known [9] how to derive on-shell kinetic (Boltzmann) equations from truncations of the 2PI effective action and one can compare the self-consistent 2PI dynamics with dynamics from kinetic theory [10–12]. However, this again serves more as a test of kinetic theory than of the 2PI truncation. Another possibility, relevant for the dynamics at very late times, is to study transport coefficients from the 2PI effective action, which gives insight into what scattering processes are included [13,14].

When the exact, untruncated evolution is accessible, one may carry out a direct comparison. This option is available in quantum mechanics, where the dynamics from the 2PI effective action can be benchmarked against the numerical solution of the Schrödinger equation [15]. Finally, perhaps the most detailed comparison has been made within classical statistical field theory, where direct numerical simulations are straightforward [5]. Moreover, the 2PI formalism can be easily applied to classical dynamics of

*Electronic address: g.aarts@swan.ac.uk†Electronic address: a.tranberg@damtp.cam.ac.uk

an initial nonequilibrium ensemble [16–19]. In Ref. [16] it was found in the context of the $1 + 1$ dimensional $O(N)$ model that the nonperturbative classical evolution, obtained numerically, is well reproduced by the 2PI-1/ N expansion at NLO for N larger than about 10, providing direct support for the use of the 2PI-1/ N approximation at NLO.

Ideally, within a given approximation scheme, the validity of a truncation is estimated by extending the method to the next order in the expansion and test for effective convergence. Because of the absence of scattering in mean-field approximations, it is essential to go to NLO and compare NLO with approximations that go further. In the coupling expansion, a first attempt to do this was made in Ref. [8]. Here it was noted that in the broken phase of a $\lambda\phi^4$ theory two diagrams contribute at $\mathcal{O}(\lambda)$: the Hartree and the background field dependent diagram, shown in Fig. 1 on the left. Perturbatively neither of these diagrams leads to (on-shell) damping, but after the self-consistent 2PI resummation the second one does. This approximation can then be extended by inclusion of the basketball diagram, shown in Fig. 1 on the right. From a comparison between the dynamical evolution in the two truncations, it was found that equilibration times differ, but only by a factor less than two, see Ref. [8] for more details. Both truncations are at the level of complexity of the 2PI-1/ N expansion to NLO and are therefore numerically tractable. Technically, the common feature of these truncations, and in fact of all truncations treated so far, is the absence of internal vertices in self-energies. This is important from a numerical point of view, which is complicated due to the presence of memory integrals in the evolution equations. Additional vertices require extra memory integrals to be carried out, which is numerically expensive.

In this paper we extend the analysis and include for the first time self-energies with internal vertices, using the framework of the 2PI-1/ N expansion to next-to-next-to-leading order (N^2 LO) in the symmetric phase of the $O(N)$ model. This opens up the possibility to make a quantitative comparison between evolution at NLO and N^2 LO in the $1/N$ expansion. The N^2 LO effective equations of motion contain additional (nested) space-time integrals for each time step, when compared to NLO. It is beyond the scope of this paper to solve those equations in full field theory. For the sake of illustration we instead specialize to quantum mechanics which allows us to test the consistency of the equations, the conservation of energy and effective convergence of the expansion. We stress that the dynamics of quantum mechanics is of course very different from field

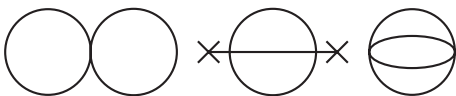


FIG. 1. Weak-coupling expansion of the 2PI effective action in the broken phase of a scalar $\lambda\phi^4$ theory [8].

theory. Given sufficient computer power the evolution equations can readily be implemented in field theory.

The paper is organized as follows. In the next section we briefly review the 2PI-1/ N expansion in the $O(N)$ model, following closely the discussion and notation of Ref. [20]. In Sec. III we present the dynamical equations to N^2 LO and give explicitly (part of) the statistical and spectral self-energies, which are much more involved than at NLO due to the presence of internal vertices. Results from the numerical implementation for the $0 + 1$ dimensional case are shown in Sec. IV, while the outlook is given in Sec. V. In three appendices we collect technicalities related to the standard loop expansion, multiloop contour integrals and the numerical solution of the Schrödinger equation.

II. 2PI-1/ N EXPANSION

Throughout the paper we consider an N component scalar field in the $O(N)$ symmetric phase ($\langle\phi_a\rangle = 0$). The action is

$$S = - \int_C d^4x \left[\frac{1}{2} \partial_\mu \phi_a \partial^\mu \phi_a + \frac{1}{2} m^2 \phi_a \phi_a + \frac{\lambda}{4!N} (\phi_a \phi_a)^2 \right], \quad (2.1)$$

with $a = 1, \dots, N$. Doubled indices are summed over. As appropriate to an out-of-equilibrium treatment, the fields are defined along the Keldysh contour \mathcal{C} in the complex-time plane, see Appendix B. The 2PI effective action depends on the full two-point function G of the theory and can be parametrized as [21]

$$\Gamma[G] = \frac{i}{2} \text{Tr} \ln G^{-1} + \frac{i}{2} \text{Tr} G_0^{-1} (G - G_0) + \Gamma_2[G], \quad (2.2)$$

where G_0^{-1} denotes the free inverse propagator. Variation of the effective action with respect to G results in the Schwinger-Dyson equation for the two-point function, $G^{-1} = G_0^{-1} - \Sigma$, which after multiplication with G reads

$$- [\square_x + m^2] G_{ab}(x, y) = i \int_z \Sigma_{ac}(x, z) G_{cb}(z, y) + i \delta_{ab} \delta_C(x - y). \quad (2.3)$$

Here we used the short-hand notation

$$\int_z = \int_C d^4z. \quad (2.4)$$

The self-energy is given by

$$\Sigma_{ab} = 2i \frac{\delta \Gamma_2[G]}{\delta G_{ab}}. \quad (2.5)$$

The full four-point function is represented by the nonlocal term on the right-hand side (RHS) of Eq. (2.3). For future reference we note here that

$$\frac{\lambda}{6N} \langle \phi_a^2(x) \phi_c^2(x) \rangle = i \int_C d^4 z \Sigma_{ac}(x, z) G_{ca}(z, x), \quad (2.6)$$

which can be verified using e.g. the Heisenberg equations of motion.

To implement the $1/N$ expansion efficiently, it is convenient to use the auxiliary-field formalism [20,22–24]. The action then reads

$$S[\phi, \chi] = - \int_x \left[\frac{1}{2} \partial_\mu \phi_a \partial^\mu \phi_a + \frac{1}{2} m^2 \phi_a \phi_a - \frac{3N}{2\lambda} \chi^2 + \frac{1}{2} \chi \phi_a \phi_a \right]. \quad (2.7)$$

Integrating out χ yields the original action (2.1). The 2PI effective action is now written in terms of the one-point function $\bar{\chi} = \langle \chi(x) \rangle$ and the two-point functions

$$\begin{aligned} G_{ab}(x, y) &= \langle T_C \phi_a(x) \phi_b(y) \rangle, \\ D(x, y) &= \langle T_C \chi(x) \chi(y) \rangle - \langle \chi(x) \rangle \langle \chi(y) \rangle, \end{aligned} \quad (2.8)$$

and reads

$$\begin{aligned} \Gamma[G, D, \bar{\chi}] &= S[0, \bar{\chi}] + \frac{i}{2} \text{Tr} \ln G^{-1} + \frac{i}{2} \text{Tr} G_0^{-1} (G - G_0) \\ &+ \frac{i}{2} \text{Tr} \ln D^{-1} + \frac{i}{2} \text{Tr} D_0^{-1} (D - D_0) \\ &+ \Gamma_2[G, D]. \end{aligned} \quad (2.9)$$

Since we take $\langle \phi_a \rangle = 0$, there is no mixing between the ϕ and χ propagators [20,22]. The free inverse propagators read

$$\begin{aligned} G_{0,ab}^{-1}(x, y) &= i[\square_x + m^2 + \bar{\chi}(x)] \delta_{ab} \delta_C(x - y), \\ D_0^{-1}(x, y) &= \frac{3N}{i\lambda} \delta_C(x - y). \end{aligned} \quad (2.10)$$

The evolution equations for the propagators G and D and the one-point function $\bar{\chi}$ are obtained by extremizing (2.9) and read

$$\begin{aligned} -[\square_x + m^2 + \bar{\chi}(x)] G_{ab}(x, y) \\ = i \int_z \Sigma_{ac}(x, z) G_{cb}(z, y) + i \delta_{ab} \delta_C(x - y), \\ \frac{3N}{\lambda} D(x, y) = i \int_z \Pi(x, z) D(z, y) + i \delta_C(x - y), \end{aligned} \quad (2.11)$$

and

$$\bar{\chi}(x) = \frac{\lambda}{6N} G_{cc}(x, x). \quad (2.12)$$

The self-energies are defined by

$$\Sigma_{ab} = 2i \frac{\delta \Gamma_2[G, D]}{\delta G_{ab}}, \quad \Pi = 2i \frac{\delta \Gamma_2[G, D]}{\delta D}. \quad (2.13)$$

It is convenient to separate the local part of D [20] and write

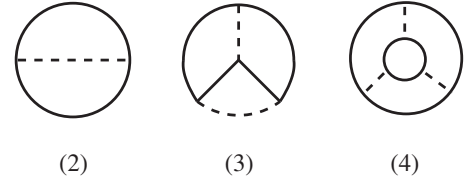


FIG. 2. NLO (2 loops) and N²LO (3 and 4 loops) contributions in the 2PI-1/ N expansion. The scalar propagator G is denoted with the full line and the auxiliary-field propagator D with the dashed line.

$$D(x, y) = \frac{\lambda}{3N} [i \delta_C(x - y) + \hat{D}(x, y)], \quad (2.14)$$

such that \hat{D} is determined from

$$\hat{D}(x, y) = -\frac{\lambda}{3N} \Pi(x, y) + \frac{i\lambda}{3N} \int_z \Pi(x, z) \hat{D}(z, y). \quad (2.15)$$

We now continue with the 2PI-1/ N expansion, in which there is one diagram at NLO and two diagrams at N²LO, see Fig. 2. For a detailed powercounting discussion we refer to Ref. [20]. It suffices here to say that a closed scalar propagator $G \sim N$ and the auxiliary-field propagator $D \sim 1/N$. It is then easy to see that diagram (2) ~ 1 and diagrams (3) and (4) $\sim 1/N$. The expressions are

$$\begin{aligned} \Gamma_2^{\text{NLO}}[G, D] &= \frac{i}{4} \int_{xy} G_{ab}^2(x, y) D(x, y), \\ \Gamma_2^{\text{NNLO}^{(3)}}[G, D] &= -\frac{i}{8} \int_{xyzw} G_{ab}(x, y) G_{bc}(y, z) G_{cd}(z, w) \\ &\quad \times G_{da}(w, x) D(x, z) D(y, w), \\ \Gamma_2^{\text{NNLO}^{(4)}}[G, D] &= \frac{i}{12} \int_{xyzx'y'z'} G_{ab}(x, y) G_{bc}(y, z) G_{ca}(z, x) \\ &\quad \times G_{a'b'}(x', y') G_{b'c'}(y', z') G_{c'a'}(z', x') \\ &\quad \times D(x, x') D(y, y') D(z, z'). \end{aligned} \quad (2.16)$$

The corresponding self-energies are shown in Figs. 3 and 4.

We continue with the $O(N)$ symmetric case, such that $G_{ab}(x, y) = G(x, y) \delta_{ab}$ and $\Sigma_{ab}(x, y) = \Sigma(x, y) \delta_{ab}$. For notational simplicity we label the self-energies according to the number of loops, e.g. $\Sigma^{(\ell)}$, where $\ell = 1, 2, 3$. We stress that the 2PI-1/ N expansion does not coincide with loop expansion in the auxiliary-field formalism. For instance, there are two more four-loop diagrams, see Fig. 5,

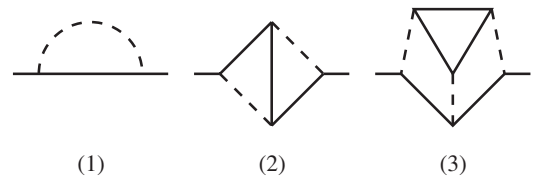


FIG. 3. Self-energy Σ at NLO (1 loop) and N²LO (2 and 3 loops).

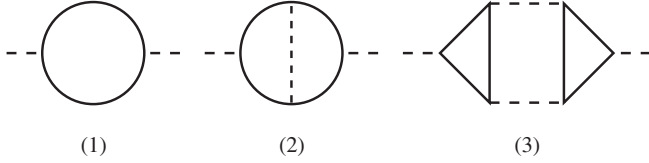


FIG. 4. Auxiliary-field self-energy Π at NLO (1 loop) and N²LO (2 and 3 loops).

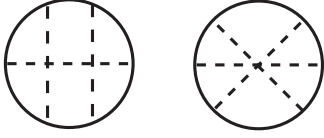


FIG. 5. Loop expansion in the auxiliary-field formalism: additional four-loop diagrams, of order $1/N^2$ (N³LO).

which only contribute at N³LO. The connection with the standard loop expansion is discussed further in Appendix A.

At NLO the self-energies read

$$\Sigma^{(1)}(x, y) = -G(x, y)D(x, y), \quad (2.17)$$

$$\Pi^{(1)}(x, y) = -\frac{N}{2}G^2(x, y), \quad (2.18)$$

and at N²LO

$$\Sigma^{(2)}(x, y) = \int_{zw} G(x, w)G(w, z)G(z, y)D(x, z)D(w, y), \quad (2.19)$$

$$\begin{aligned} \Sigma^{(3)}(x, y) &= -N \int_{zx'y'z'} G(x, z)G(z, y)G(x', y')G(y', z') \\ &\quad \times G(z', x')D(x, x')D(y, y')D(z, z'), \\ \Pi^{(2)}(x, y) &= \frac{N}{2} \int_{zw} G(x, w)G(w, y)G(x, z)G(z, y)D(z, w), \\ \Pi^{(3)}(x, y) &= -\frac{N^2}{2} \int_{zz'ww'} G(x, z)G(z, w)G(w, x)G(y, z') \\ &\quad \times G(z', w')G(w', y)D(w, w')D(z, z'). \end{aligned} \quad (2.20)$$

III. CAUSAL EQUATIONS

To bring the evolution equations in a form that can be solved numerically, the contour propagators and self-energies are written in terms of statistical (F) and spectral (ρ) components [25],

$$G(x, y) = F(x, y) - \frac{i}{2} \text{sgn}_c(x, y)\rho(x, y), \quad (3.1)$$

and similar for \hat{D} , Σ and Π . Here $\text{sgn}_c(x, y) = \Theta_c(x^0 - y^0) - \Theta_c(y^0 - x^0)$ is the sign function along the contour, see Appendix B. The explicitly causal equations then read

[20]

$$\begin{aligned} [\square_x + M^2(x)]\rho(x, y) &= - \int_{y^0}^{x^0} dz \Sigma_\rho(x, z)\rho(z, y), \\ [\square_x + M^2(x)]F(x, y) &= - \int_0^{x^0} dz \Sigma_\rho(x, z)F(z, y) \\ &\quad + \int_0^{y^0} dz \Sigma_F(x, z)\rho(z, y), \end{aligned} \quad (3.2)$$

where

$$M^2(x) = m^2 + \lambda \frac{N+2}{6N} F(x, x), \quad (3.3)$$

and

$$\begin{aligned} \frac{3N}{\lambda} \hat{D}_\rho(x, y) &= -\Pi_\rho(x, y) + \int_{y^0}^{x^0} dz \Pi_\rho(x, z)\hat{D}_\rho(z, y), \\ \frac{3N}{\lambda} \hat{D}_F(x, y) &= -\Pi_F(x, y) + \int_0^{x^0} dz \Pi_\rho(x, z)\hat{D}_F(z, y) \\ &\quad - \int_0^{y^0} dz \Pi_F(x, z)\hat{D}_\rho(z, y). \end{aligned} \quad (3.4)$$

We use here the notation

$$\int_{y^0}^{x^0} dz = \int_{y^0}^{x^0} dz^0 \int d^3z. \quad (3.5)$$

Equations of motion derived from truncations of the 2PI effective action conserve the following energy functional [cf. Eq. (2.6)],

$$\begin{aligned} E/N &= \int d^3x \frac{1}{2} \left[\partial_{x^0} \partial_{y^0} + \partial_{x^i} \partial_{y^i} + m^2 \right. \\ &\quad \left. + \frac{\lambda}{12} \frac{N+2}{N} F(x, x) \right] F(x, y) \Big|_{x=y} \\ &\quad + \frac{1}{4} \int d^3x \int_0^{x^0} dz^0 \int d^3z [\Sigma_\rho(x, z)F(z, x) \\ &\quad - \Sigma_F(x, z)\rho(z, x)]. \end{aligned} \quad (3.6)$$

The statistical and spectral self-energies at NLO can be found in Ref. [20] and read

$$\begin{aligned} \Sigma_F^{(1)}(x, y) &= -\frac{\lambda}{3N} \left[F(x, y)\hat{D}_F(x, y) - \frac{1}{4}\rho(x, y)\hat{D}_\rho(x, y) \right], \\ \Sigma_\rho^{(1)}(x, y) &= -\frac{\lambda}{3N} [\rho(x, y)\hat{D}_F(x, y) + F(x, y)\hat{D}_\rho(x, y)], \\ \Pi_F^{(1)}(x, y) &= -\frac{N}{2} \left[F(x, y)F(x, y) - \frac{1}{4}\rho(x, y)\rho(x, y) \right], \\ \Pi_\rho^{(1)}(x, y) &= -NF(x, y)\rho(x, y). \end{aligned} \quad (3.7)$$

We now come to the causal self-energies at N²LO. These self-energies have internal vertices and therefore require further contour integrals. We start by discussing $\Sigma^{(2)}(x, y)$ in some detail. Since we have separated the local part of D , we first insert Eq. (2.14) into Eq. (2.19). This yields

$$\begin{aligned}
\Sigma^{(2)}(x, y) &= \int_{zw} D(x, z)G(x, w)G(y, z)D(y, w)G(z, w) \\
&= -g^2 G^3(x, y) + ig^2 \int_z [\hat{D}(x, z)G(x, y)G^2(y, z) \\
&\quad + G^2(x, z)G(x, y)\hat{D}(y, z)] \\
&\quad + g^2 \int_{zw} \hat{D}(x, z)G(x, w)G(y, z)\hat{D}(y, w)G(z, w),
\end{aligned} \tag{3.8}$$

where

$$g = \frac{\lambda}{3N}. \tag{3.9}$$

This is naturally organized according to the number of \hat{D} propagators and we use the notation $\Sigma^{(2,n)}$ for the contribution with n \hat{D} 's. The term without \hat{D} propagators is the N²LO contribution to the setting-sun diagram and reads

$$\begin{aligned}
\Sigma_F^{(2,0)}(x, y) &= -g^2 \left[F^2(x, y) - \frac{3}{4} \rho^2(x, y) \right] F(x, y), \\
\Sigma_\rho^{(2,0)}(x, y) &= -g^2 \left[3F^2(x, y) - \frac{1}{4} \rho^2(x, y) \right] \rho(x, y).
\end{aligned} \tag{3.10}$$

The other terms quickly become rather lengthy, so we first discuss the general structure. Every line in the self-energy can be either a statistical (F) or a spectral (ρ) function.

With L lines, this gives a maximum of 2^L possibilities. However, in order to find a nonzero result, every internal vertex needs at least one sgn function coming from a ρ -type line ending on it (see Appendix B). This implies that a diagram with V internal vertices should have at least V ρ -type lines. This reduces the maximal number of terms in the expressions for the causal diagrams to

$$\# \text{ distinct contributions} \leq \sum_{l_\rho=V}^L \binom{L}{l_\rho} \leq 2^L, \tag{3.11}$$

where l_ρ is the number of ρ -type lines. The actual number of nonzero contributions is in fact slightly less, since some contributions vanish after performing the contour integrals, due to the appearance of internal vertices without ρ -type lines (even though $l_\rho \geq V$). Finally, the number of terms that have to be independently evaluated is further reduced due to the fact that statistical (spectral) self-energies are explicitly even (odd) under interchange of x and y . We also note that if the contour self-energy is proportional to i (such as $\Sigma^{(2,1)}$), expressions with an odd number of ρ -type lines contribute to Σ_F and expressions with an even number of ρ -type lines to Σ_ρ . If the contour self-energy is proportional to 1 (such as $\Sigma^{(2,2)}$), this is reversed.

Using the contour integration rules summarized in Appendix B, we find explicitly

$$\begin{aligned}
\frac{1}{g^2} \Sigma_F^{(2,1)}(x, y) &= + \int_0^x dz \left[2F(x, z)\rho(x, z)\hat{D}_F(y, z) + \hat{D}_\rho(x, z) \left(F^2(y, z) - \frac{1}{4} \rho^2(y, z) \right) \right] F(x, y) \\
&\quad + \int_0^y dz \left[2\hat{D}_F(x, z)F(y, z)\rho(y, z) + \left(F^2(x, z) - \frac{1}{4} \rho^2(x, z) \right) \hat{D}_\rho(y, z) \right] F(x, y) \\
&\quad + \int_y^x dz \frac{1}{2} \left[\hat{D}_\rho(x, z)F(y, z)\rho(y, z) + F(x, z)\rho(x, z)\hat{D}_\rho(y, z) \right] \rho(x, y),
\end{aligned} \tag{3.12}$$

and

$$\begin{aligned}
\frac{1}{g^2} \Sigma_\rho^{(2,1)}(x, y) &= + \int_0^x dz \left[2F(x, z)\rho(x, z)\hat{D}_F(y, z) + \hat{D}_\rho(x, z) \left(F^2(y, z) - \frac{1}{4} \rho^2(y, z) \right) \right] \rho(x, y) \\
&\quad + \int_0^y dz \left[2\hat{D}_F(x, z)F(y, z)\rho(y, z) + \left(F^2(x, z) - \frac{1}{4} \rho^2(x, z) \right) \hat{D}_\rho(y, z) \right] \rho(x, y) \\
&\quad - \int_y^x dz 2 \left[\hat{D}_\rho(x, z)F(y, z)\rho(y, z) + F(x, z)\rho(x, z)\hat{D}_\rho(y, z) \right] F(x, y),
\end{aligned} \tag{3.13}$$

and for the self-energy with two \hat{D} propagators

$$\begin{aligned}
\frac{1}{g^2} \Sigma_F^{(2,2)}(x, y) = & - \int_0^x dz \int_0^x dw \rho(x, z) \hat{D}_\rho(x, w) \hat{D}_F(y, z) F(y, w) F(z, w) \\
& - \int_0^y dz \int_0^y dw \hat{D}_F(x, z) F(x, w) \rho(y, z) \hat{D}_\rho(y, w) F(z, w) \\
& - \int_0^x dz \int_0^z dw [\rho(x, z) \hat{D}_F(x, w) \hat{D}_F(y, z) F(y, w) + \hat{D}_F(x, z) F(x, w) F(y, z) \hat{D}_\rho(y, w)] \rho(z, w) \\
& - \int_0^y dz \int_0^z dw [\hat{D}_F(x, z) F(x, w) \rho(y, z) \hat{D}_F(y, w) + F(x, z) \hat{D}_\rho(x, w) \hat{D}_F(y, z) F(y, w)] \rho(z, w) \\
& - \int_0^x dz \int_0^y dw [\hat{D}_\rho(x, z) F(x, w) F(y, z) \hat{D}_\rho(y, w) + \rho(x, z) \hat{D}_F(x, w) \hat{D}_F(y, z) \rho(y, w)] F(z, w) \\
& - \int_0^x dz \int_z^y dw \frac{1}{4} [\hat{D}_\rho(x, z) F(x, w) \rho(y, z) \hat{D}_\rho(y, w) + \rho(x, z) \hat{D}_F(x, w) \hat{D}_\rho(y, z) \rho(y, w)] \rho(z, w) \\
& - \int_0^y dz \int_z^x dw \frac{1}{4} [\hat{D}_\rho(x, z) \rho(x, w) \rho(y, z) \hat{D}_F(y, w) + \rho(x, z) \hat{D}_\rho(x, w) \hat{D}_\rho(y, z) F(y, w)] \rho(z, w) \\
& + \int_y^x dz \int_y^x dw \frac{1}{4} \hat{D}_\rho(x, z) \rho(x, w) \rho(y, z) \hat{D}_\rho(y, w) F(z, w), \tag{3.14}
\end{aligned}$$

and

$$\begin{aligned}
\frac{1}{g^2} \Sigma_\rho^{(2,2)}(x, y) = & + \int_y^x dz \int_0^x dw [\hat{D}_\rho(x, z) \rho(x, w) \rho(y, z) \hat{D}_F(y, w) + \rho(x, z) \hat{D}_\rho(x, w) \hat{D}_\rho(y, z) F(y, w)] F(z, w) \\
& + \int_y^x dz \int_0^y dw [\hat{D}_\rho(x, z) F(x, w) \rho(y, z) \hat{D}_\rho(y, w) + \rho(x, z) \hat{D}_F(x, w) \hat{D}_\rho(y, z) \rho(y, w)] F(z, w) \\
& + \int_y^x dz \int_0^z dw [\hat{D}_\rho(x, z) F(x, w) \rho(y, z) \hat{D}_F(y, w) + \rho(x, z) \hat{D}_F(x, w) \hat{D}_\rho(y, z) F(y, w)] \rho(z, w) \\
& + \int_y^x dz \int_y^z dw \frac{1}{2} [\hat{D}_\rho(x, z) F(x, w) F(y, z) \hat{D}_\rho(y, w) + \rho(x, z) \hat{D}_F(x, w) \hat{D}_F(y, z) \rho(y, w)] \rho(z, w) \\
& + \int_y^x dz \int_x^z dw \frac{1}{2} [F(x, z) \hat{D}_\rho(x, w) \hat{D}_\rho(y, z) F(y, w) + \hat{D}_F(x, z) \rho(x, w) \rho(y, z) \hat{D}_F(y, w)] \rho(z, w) \\
& - \int_y^x dz \int_0^y dw \frac{1}{4} [\hat{D}_\rho(x, z) \rho(x, w) \rho(y, z) \hat{D}_\rho(y, w) + \rho(x, z) \hat{D}_\rho(x, w) \hat{D}_\rho(y, z) \rho(y, w)] \rho(z, w). \tag{3.15}
\end{aligned}$$

In a few terms we used the symmetry of the integrand to make some minor simplifications.

For the auxiliary-field self-energy we proceed in the same manner and find, at two loops,

$$\begin{aligned}
\Pi^{(2)}(x, y) = & \frac{N}{2} \int_{zw} G(x, z) G(x, w) G(y, z) G(y, w) D(z, w) \\
= & \frac{i\lambda}{6} \int_z G^2(x, z) G^2(y, z) + \frac{\lambda}{6} \int_{zw} G(x, z) G(x, w) G(y, z) G(y, w) \hat{D}(z, w). \tag{3.16}
\end{aligned}$$

Denoting these diagrams again as $\Pi^{(2,n)}$, where n denotes the number of \hat{D} propagators, we find with $n = 0$,

$$\begin{aligned}
\Pi_F^{(2,0)}(x, y) = & + \frac{\lambda}{3} \int_0^x dz F(x, z) \rho(x, z) \left(F^2(y, z) - \frac{1}{4} \rho^2(y, z) \right) + \frac{\lambda}{3} \int_0^y dz \left(F^2(x, z) - \frac{1}{4} \rho^2(x, z) \right) F(y, z) \rho(y, z), \\
\Pi_\rho^{(2,0)}(x, y) = & - \frac{2\lambda}{3} \int_y^x dz F(x, z) \rho(x, z) F(y, z) \rho(y, z), \tag{3.17}
\end{aligned}$$

and with one \hat{D} propagator

$$\begin{aligned}
\frac{6}{\lambda} \Pi_F^{(2,1)}(x, y) = & - \int_0^x dz \int_0^x dw \rho(x, z) \rho(x, w) F(y, z) F(y, w) \hat{D}_F(z, w) \\
& - \int_0^y dz \int_0^y dw F(x, z) F(x, w) \rho(y, z) \rho(y, w) \hat{D}_F(z, w) \\
& - \int_0^x dz \int_0^z dw 2\rho(x, z) F(x, w) F(y, z) F(y, w) \hat{D}_\rho(z, w) \\
& - \int_0^y dz \int_0^z dw 2F(x, z) F(x, w) \rho(y, z) F(y, w) \hat{D}_\rho(z, w) \\
& - \int_0^x dz \int_0^y dw 2\rho(x, z) F(x, w) F(y, z) \rho(y, w) \hat{D}_F(z, w) \\
& + \int_y^x dz \int_y^x dw \frac{1}{4} \rho(x, z) \rho(x, w) \rho(y, z) \rho(y, w) \hat{D}_F(z, w) \\
& - \int_0^x dz \int_z^y dw \frac{1}{2} \rho(x, z) F(x, w) \rho(y, z) \rho(y, w) \hat{D}_\rho(z, w) \\
& - \int_0^y dz \int_z^x dw \frac{1}{2} \rho(x, z) \rho(x, w) \rho(y, z) F(y, w) \hat{D}_\rho(z, w), \tag{3.18}
\end{aligned}$$

and

$$\begin{aligned}
\frac{6}{\lambda} \Pi_\rho^{(2,1)}(x, y) = & + \int_y^x dz \int_0^x dw 2\rho(x, z) \rho(x, w) \rho(y, z) F(y, w) \hat{D}_F(z, w) \\
& + \int_y^x dz \int_0^y dw 2\rho(x, z) F(x, w) \rho(y, z) \rho(y, w) \hat{D}_F(z, w) \\
& + \int_y^x dz \int_y^z dw \rho(x, z) F(x, w) F(y, z) \rho(y, w) \hat{D}_\rho(z, w) \\
& + \int_y^x dz \int_x^z dw F(x, z) \rho(x, w) \rho(y, z) F(y, w) \hat{D}_\rho(z, w) \\
& + \int_y^x dz \int_0^z dw 2\rho(x, z) F(x, w) \rho(y, z) F(y, w) \hat{D}_\rho(z, w) \\
& - \int_y^x dz \int_0^y dw \frac{1}{2} \rho(x, z) \rho(x, w) \rho(y, z) \rho(y, w) \hat{D}_\rho(z, w). \tag{3.19}
\end{aligned}$$

Since the Π self-energies have more internal symmetry than the Σ self-energies, the corresponding expressions are slightly shorter. We also emphasize that for nonequilibrium quantum fields statistical (F) and spectral (ρ) components are independent [25]: there are therefore no (obvious) cancellations between the various terms above.

We now briefly discuss the requirements for a numerical solution. The evolution equations for the two-point functions (3.2) and (3.4) can be solved numerically by discretization on a space-time lattice. For this it is necessary to perform the space-time integrals on the RHS of those equations. This has been discussed extensively in references cited in Ref. [7]. At NLO, the self-energies (3.7) are simple products of F , ρ , \hat{D}_F and \hat{D}_ρ . At N^2 LO however, the self-energies themselves require space-time integrals to be performed: the two-loop self-energy presented above contains up to two internal vertices, and the three-loop self-energy will contain up to four internal vertices. These lead to nested loops over time, dramatically increasing the necessary CPU time. Because of the obvious numerical

effort required, we have not attempted to solve the full N^2 LO approximation. Instead we concentrate in the next section on the three-loop approximation (two-loop self-energy) in the $0 + 1$ dimensional case.

The statistical and spectral self-energies corresponding to the three-loop self-energies $\Sigma^{(3)}$ and $\Pi^{(3)}$ in Eqs. (2.19) and (2.20) are very lengthy. For instance, for $\Sigma_F^{(3,3)}$ one has to consider 44 distinct nonzero diagrams which differ in the way the statistical and spectral functions appear on the 8 internal lines. Because we are not including these diagrams in the numerical analysis below, we refrain from giving the explicit expressions. Using the contour integrals listed in Appendix B it is straightforward, albeit cumbersome, to work them out.

IV. QUANTUM DYNAMICS

Since a numerical solution of the full $3 + 1$ dimensional field theory seems intractable, we now restrict our attention to quantum mechanics, which in this context is equivalent

to 0 + 1 dimensional field theory. We consider the Hamiltonian

$$\mathcal{H} = \frac{1}{2} p_a p_a + \frac{1}{2} m^2 q_a q_a + \frac{\lambda}{4! N} (q_a q_a)^2, \quad (4.1)$$

and consider $O(N)$ symmetric Gaussian initial conditions, parametrized by the normalized Gaussian density matrix [26],

$$\begin{aligned} \langle q' | \hat{\rho}(\eta, \xi, \sigma) | q \rangle = & \frac{1}{(2\pi\xi^2)^{N/2}} \exp \left[-\frac{\sigma^2 + 1}{8\xi^2} (q_a^2 + q_a'^2) \right. \\ & \left. + i \frac{\eta}{2\xi} (q_a^2 - q_a'^2) + \frac{\sigma^2 - 1}{4\xi^2} q_a q_a' \right]. \end{aligned} \quad (4.2)$$

Recall that we consider $\langle q_a \rangle = \langle p_a \rangle = 0$. When $\sigma = 1$, this reduces to the density matrix of a pure state,

$$\hat{\rho}(\eta, \xi, 0) = |\Psi_0\rangle\langle\Psi_0|, \quad (4.3)$$

with

$$\Psi_0(q) = \langle q | \Psi_0 \rangle = \frac{1}{(2\pi\xi^2)^{N/4}} \exp \left[-\left(\frac{1}{4\xi^2} + i \frac{\eta}{2\xi} \right) q_a^2 \right]. \quad (4.4)$$

In this case, the Schrödinger equation

$$i \frac{\partial}{\partial t} \Psi(q_a, t) = \mathcal{H} \Psi(q_a, t), \quad (4.5)$$

can be solved numerically (see Appendix C), which allows for a comparison with the untruncated evolution [15,27].

The expressions from the previous sections remain unchanged, provided that all reference to space indices and integrals are dropped, e.g.,

$$\begin{aligned} F_{ab}(x, y) & \rightarrow F_{ab}(t, t') = \delta_{ab} F(t, t') \\ & = \frac{1}{2} \langle q_a(t) q_b(t') + q_b(t') q_a(t) \rangle, \end{aligned} \quad (4.6)$$

$$\rho_{ab}(x, y) \rightarrow \rho_{ab}(t, t') = \delta_{ab} \rho(t, t') = i \langle [q_a(t), q_b(t')] \rangle. \quad (4.7)$$

The density matrix (4.2) yields the following initial conditions for the statistical function

$$\begin{aligned} F(t, t')|_{t=t'=0} & = \xi^2, \quad \partial_t F(t, t')|_{t=t'=0} = \xi \eta, \\ \partial_t \partial_{t'} F(t, t')|_{t=t'=0} & = \left(\eta^2 + \frac{\sigma^2}{4\xi^2} \right). \end{aligned} \quad (4.8)$$

As always, the spectral function satisfies

$$\rho(t, t) = 0, \quad \partial_t \rho(t, t')|_{t=t'} = 1. \quad (4.9)$$

The initial conditions for \hat{D}_F and \hat{D}_ρ are determined by Eq. (3.4). The (conserved) energy takes the value

$$\langle \mathcal{H} \rangle / N = \frac{1}{2} \eta^2 + \frac{\sigma^2}{8\xi^2} + \frac{1}{2} m^2 \xi^2 + \frac{\lambda}{4!} \frac{N+2}{N} \xi^4. \quad (4.10)$$

We solve the evolution equations (3.2) and (3.4) numerically for various λ and N using a simple leapfrog algorithm and a standard discretization of the time integrals. We set $m = 1$ throughout. For a step size of $dt = 0.01$ the entire memory kernel fits on a 1 GB CPU, for runs until $t = 20$ (2000 time steps). Using $dt = 0.001$ leads to indistinguishable results. A run which includes the first diagram at N²LO takes about 2 days on a single 3 GHz machine, although presumably this can be improved somewhat. The CPU time grows as the number of time steps to the 4th power. A run at NLO is roughly 400 times faster. Including another nested integral (i.e. including the second N²LO diagram) is expected to give at least another factor of 400, making such an extension very challenging indeed.

In order to study the effect of the different initial conditions, we show in Fig. 6 the time evolution at NLO for $N = 8$ and $\lambda = 1$, for various choices of initial states with the same energy. The early evolution, $0 < t < 0.5$, can be understood from the uncoupled case ($\lambda = 0$), in which the dynamics is readily solved, and the two-point functions are

$$\begin{aligned} F(t, t') & = \xi^2 \cos(mt) \cos(mt') + \frac{1}{m^2} \left(\eta^2 + \frac{\sigma^2}{4\xi^2} \right) \sin(mt) \\ & \quad \times \sin(mt') + \frac{\xi \eta}{m} \sin[m(t+t')], \\ \rho(t, t') & = \frac{\sin[m(t-t')]}{m}. \end{aligned} \quad (4.11)$$

The subsequent evolution is of course very different from the free case, in which damping is absent.

We now continue with a relative large value of $\eta = 5$ and a smaller $\xi = 0.4$ (corresponding to a squeezed initial state) since this yields an initially large amplitude and subsequent strong damping effects. For the sake of comparison with the numerical solution of the Schrödinger equation, we consider from now on pure states only, $\sigma = 1$.

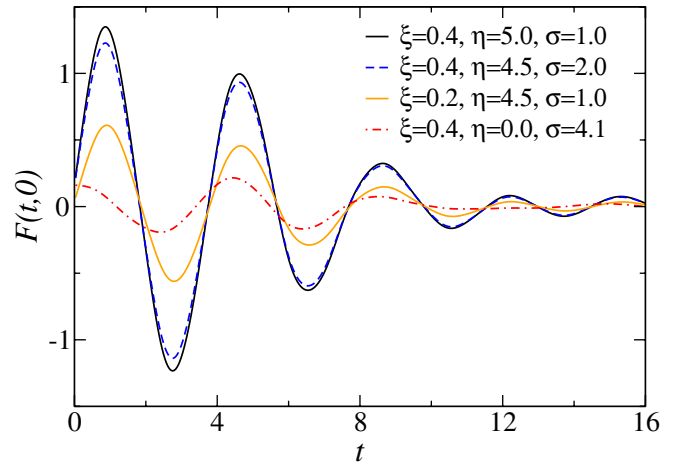


FIG. 6 (color online). Unequal time correlator $F(t, 0)$ at NLO for various choices of initial states with the same energy ($N = 8$, $\lambda = 1$).

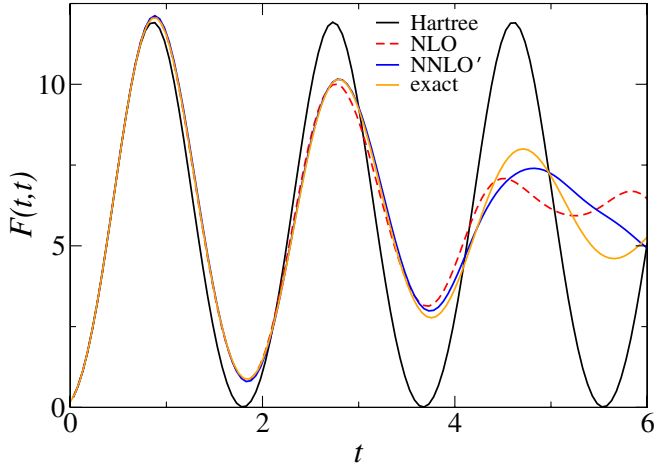


FIG. 7 (color online). Time evolution of the equal-time correlator $F(t, t)$ for various approximations and the exact result from a numerical solution of the Schrödinger equation ($N = 8, \lambda = 1, \eta = 5, \xi = 0.4, \sigma = 1$).

In Fig. 7 we show the evolution of the equal-time correlator $F(t, t)$ for the different levels of truncation, at $N = 8$. In the Hartree approximation, all nonlocal terms on the RHS of the evolution equations (3.2) are dropped and only the time-dependent mass parameter is preserved. Equations (3.4) are dropped altogether. At NLO the one-loop self-energies (3.7) without internal vertices are kept. As explained at the end of the previous section, at N²LO we only keep the two-loop self-energies, with up to two internal vertices, in addition to the one-loop self-energies. We will refer to this truncation as the N²LO' approximation. Since it is derived from the two and three-loop diagrams in Fig. 2, it is a 2PI self-consistent approximation. The result labeled with “exact” corresponds to the numerical solution of the Schrödinger equation, which is detailed in Appendix C. Energy conservation at N²LO' is demon-

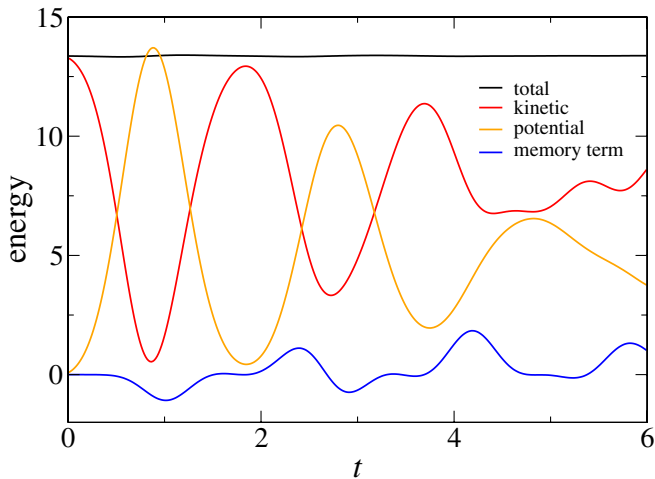


FIG. 8 (color online). Time evolution of different energy components at N²LO' (same parameters as in Fig. 7).

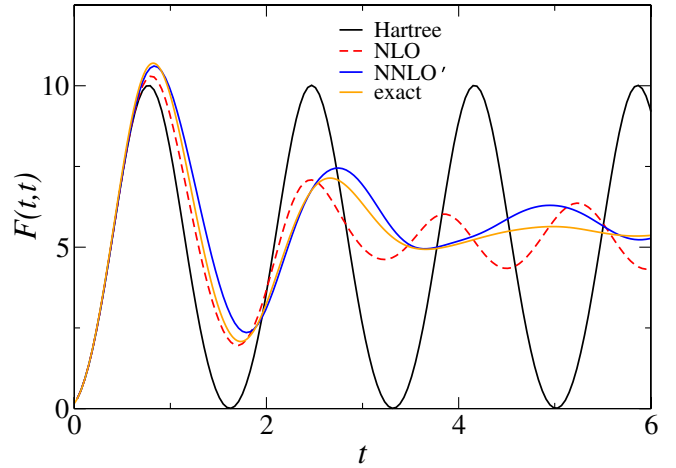


FIG. 9 (color online). Same as Fig. 7, for $N = 2$.

strated in Fig. 8, where the three components in Eq. (3.6) and their sum is shown.

A close look at Fig. 7 shows that for early times both the NLO and the N²LO' approximation are in quantitative agreement with the exact result. The amplitude in the Hartree approximation shows no sign of decreasing, due to a complete absence of dephasing in quantum mechanics [28]. Around $t = 2.7$, the NLO approximation starts to differ from the exact evolution, whereas the evolution at N²LO' is capable to follow the exact evolution a bit longer. Around $t = 4$ we find that both truncations fail to track the exact evolution and continue to evolve in an irregular fashion. We have verified that this behavior is not due to the time discretization. We also note that energy remains conserved. The irregular behavior at later times seems to be peculiar to quantum mechanics and has been observed before in dynamics from truncated effective actions [15]. As far as we know, it has not been observed in 2PI dynamics in the field theory case, where already the NLO approximation results in equilibration and thermalization. In

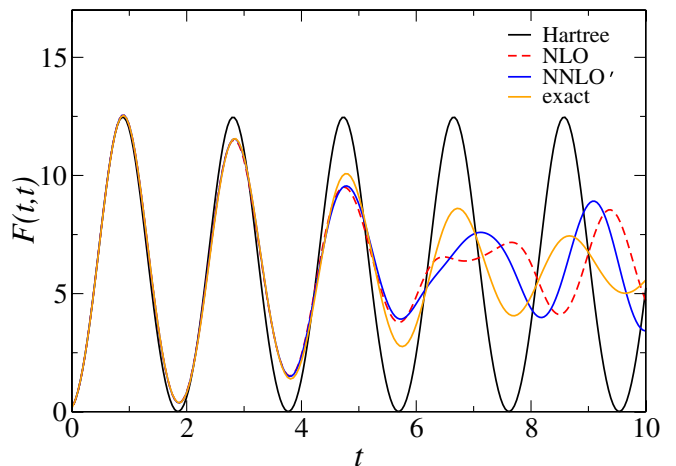


FIG. 10 (color online). Same as Fig. 7, for $N = 20$.

this sense quantum mechanics, with only a finite number of degrees of freedom, is very different.

If we continue with a comparison at early times, we note that for $N = 8$ the N^2LO' approximation works slightly better than the NLO approximation. This can be investigated further by looking at different values for N . Since the N^2LO' term is suppressed by $1/N$, it is expected that the difference between the N^2LO' and the NLO evolution will be largest for smaller N , while for larger N the $1/N$ expansion itself is better behaved and the difference between N^2LO' and NLO is reduced.

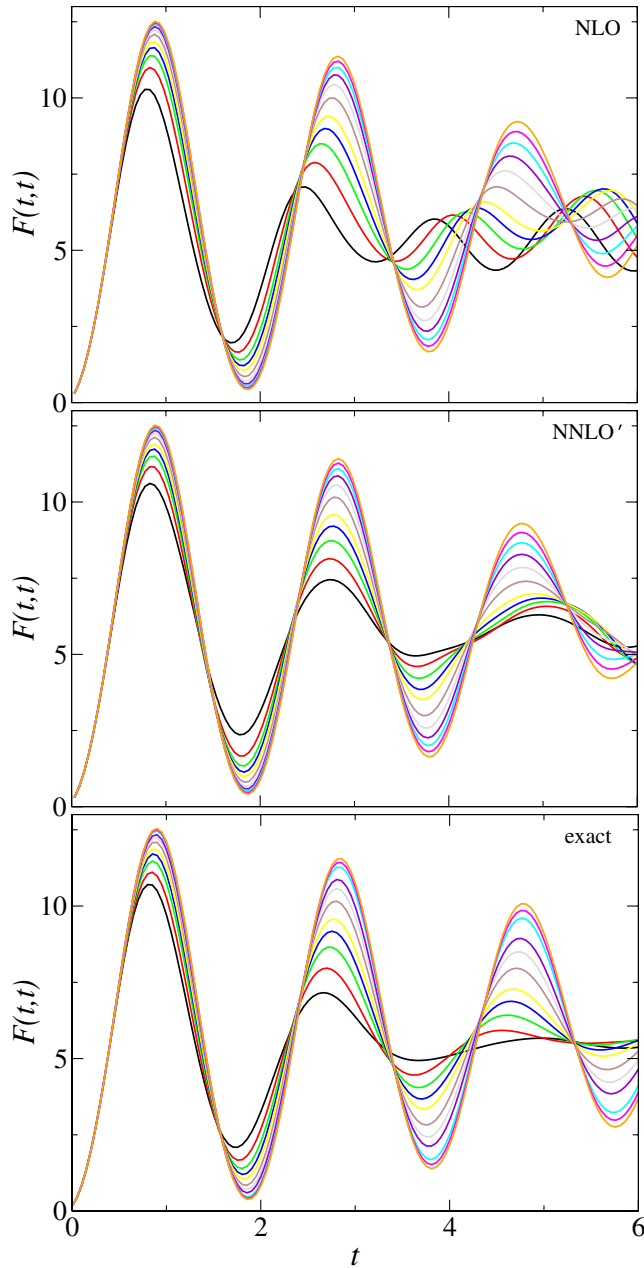


FIG. 11 (color online). Time evolution of $F(t,t)$ for NLO (upper), N^2LO' (middle) and exact (lower) dynamics for various $2 \leq N \leq 20$ (other parameters as in Fig. 7).

This qualitative picture is confirmed by first going to smaller N . In Fig. 9 we show again the equal-time correlation function, but now for $N = 2$. As expected, the evolution ceases to follow the exact one earlier, but a close look at the first maximum indicates that it is first the Hartree approximation that breaks down, subsequently the NLO approximation and finally the N^2LO' approximation. At later times irregular behavior is again observed. We find therefore that at early times an increase in the order of the truncation has a quantitatively correct effect. In Fig. 10 the equal-time correlation function is shown again, but now for larger $N = 20$. In this case the effect of adding the N^2LO' contribution is much less important, as expected, and we find that the N^2LO' evolution follows NLO rather than the exact curve, consistent with an effective convergence of the expansion for large N . Both curves follow the exact evolution for longer than in the cases shown above.

A comparison between the NLO, the N^2LO' and the exact evolution is shown in Fig. 11, for a wide range of N , from $N = 2$ to $N = 20$. It is observed that the exact

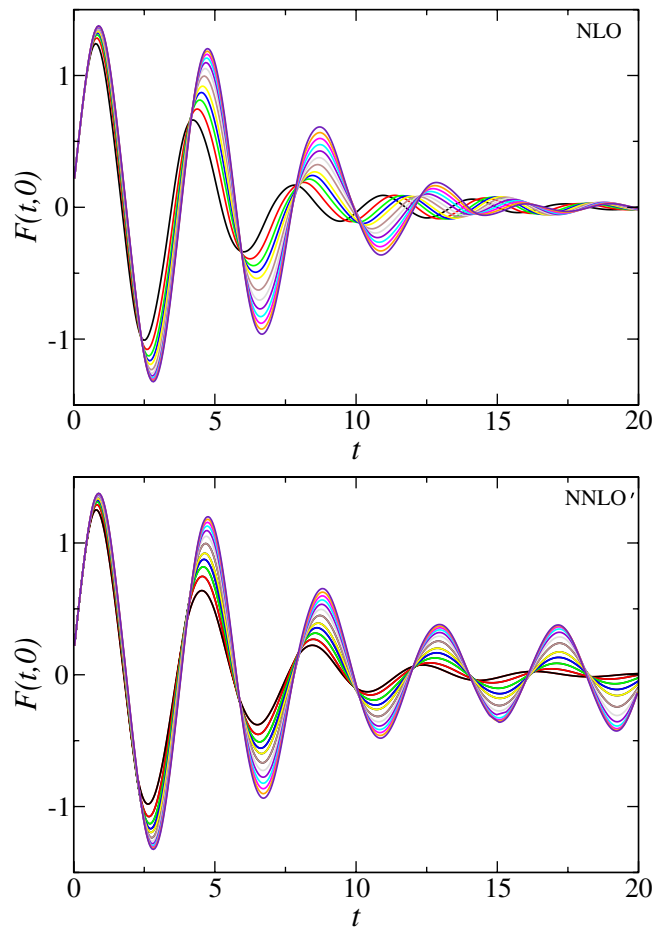


FIG. 12 (color online). Unequal time correlation function $F(t,0)$ for NLO (upper) and N^2LO' (lower) dynamics for various $2 \leq N \leq 20$ (other parameters as in Fig. 7).

solution appears to be intermediate between the NLO and $N^2\text{LO}'$ evolution, with the evolution at $N^2\text{LO}'$ performing slightly better, in particular, in terms of the oscillation frequency at smaller N .

As mentioned above, thermalization and equilibration cannot be investigated in quantum mechanics. However, in analogy with field theory effective loss of memory can be studied. In Fig. 12 we show the unequal-time two-point function $F(t, 0)$ for various values of N . Because it is nonlocal in time, this correlator is not immediately accessible from the solution of the Schrödinger equation. Smaller values of N correspond to a more rapid decrease of the amplitude, as expected. Maybe surprisingly, the memory appears to be washed out faster at NLO than at $N^2\text{LO}'$. However, this conclusion should be treated with care, since the approximations fail to track the exact evolution after some (N dependent) time, as was shown above for the equal-time correlation functions.

V. OUTLOOK

We considered nonequilibrium dynamics in the $O(N)$ model, employing the 2PI- $1/N$ expansion to $N^2\text{LO}$. We presented the explicit expressions for the three-loop approximation in the auxiliary-field formalism, to which we refer as $N^2\text{LO}'$, and indicated how to obtain to full $N^2\text{LO}$ contribution. The resulting evolution equations were solved numerically for quantum mechanics.

While the qualitative change in the nonequilibrium evolution when going from Gaussian (LO) approximations to NLO is enormous, the impact when changing from NLO to $N^2\text{LO}$ is reassuringly small. This indicates that the 2PI- $1/N$ expansion is effectively rapidly converging and that higher order effects give quantitative corrections only. We found that at early times the evolution at $N^2\text{LO}'$ performs slightly better than at NLO. This is especially visible at small N , where the higher-order contribution is not suppressed. At large times we found that all truncations break down, but we believe that this is special for quantum mechanics since it has not been observed in field theory, where already the NLO approximation has been seen to perform very well. It would therefore be very interesting to implement the $N^2\text{LO}$ truncation, or at least the three-loop diagram as we considered here, in a $1+1$ dimensional scalar $O(N)$ model and test the apparent convergence quantitatively in field theory, also for late times. Alternatively, with some effort one may also be able to do the full $N^2\text{LO}$ approximation in the case of quantum mechanics.

Finally, in this paper we only considered the symmetric phase. However, an extension to the broken phase at $N^2\text{LO}$ is straightforward, since it involves only one additional two-loop diagram in the effective action, yielding new self-energy-type contributions without internal vertices [20]. In fact, this diagram has been included already in the so-called ‘‘bare vertex approximation’’ [22].

ACKNOWLEDGMENTS

G. A. is supported by PPARC AF Grant No. PPA/A/R/2003/00278. A. T. is supported by the PPARC SPG ‘‘Classical Lattice Field Theory.’’

APPENDIX A: LOOP EXPANSION

In order to make a connection between the $1/N$ expansion and the ordinary loop expansion (see Fig. 13), we give here the expression up to five loops in the loop expansion in the $O(N)$ -symmetric case. We write the 2PI contribution as $\Gamma_2 = \sum_{l=2}^{\infty} \Gamma_2^{(l)}$ and find to fourth order

$$\Gamma_2^{(2)} = -\frac{\lambda}{8} \frac{(N+2)}{3} \int_x G^2(x, x), \quad (\text{A1})$$

$$\Gamma_2^{(3)} = \frac{i\lambda^2}{48} \frac{(N+2)}{3N} \int_{xy} G^4(x, y), \quad (\text{A2})$$

$$\Gamma_2^{(4)} = \frac{\lambda^3}{48} \frac{(N+2)(N+8)}{27N^2} \int_{xyz} G^2(x, y)G^2(x, z)G^2(z, y). \quad (\text{A3})$$

At fifth order two diagrams contribute, $\Gamma_2^{(5)} = \Gamma_2^{(5a)} + \Gamma_2^{(5b)}$, which read

$$\Gamma_2^{(5a)} = -\frac{i\lambda^4}{128} \frac{(N+2)(N^2+6N+20)}{81N^3} \int_{xyzw} G^2(x, y) \times G^2(y, z)G^2(z, w)G^2(w, x) \quad (\text{A4})$$

$$\Gamma_2^{(5b)} = -\frac{i\lambda^4}{32} \frac{(N+2)(5N+22)}{81N^3} \int_{xyzw} G^2(x, y)G(x, z) \times G(x, w)G^2(z, w)G(y, z)G(y, w). \quad (\text{A5})$$

In the 2PI- $1/N$ expansion to $N^2\text{LO}$, $\Gamma_2^{(2)}$ and $\Gamma_2^{(3)}$ are completely included, while from $\Gamma_2^{(4)}$ and $\Gamma_2^{(5a)}$ the NLO and $N^2\text{LO}$ parts are taken into account. The eye diagram

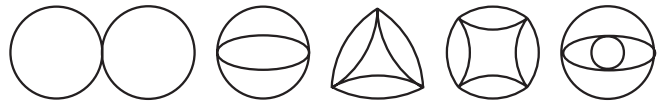


FIG. 13. Loop expansion: contribution to Γ_2 up to fifth loop order.

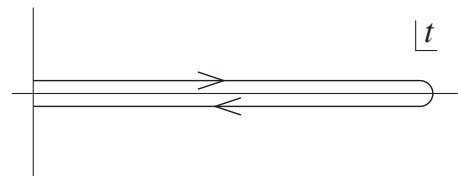


FIG. 14. Keldysh contour in the complex-time plane.

$\Gamma_2^{(5b)}$ starts at N²LO only. Part of the leading N²LO contribution is taken into account via the three-loop diagram in the auxiliary-field formalism and part via the four-loop diagram. The eye diagram is special since it is the first diagram that contributes to the bulk viscosity in the weak coupling limit [13,29].

APPENDIX B: CONTOUR INTEGRALS

The evolution equations are formulated along the Keldysh contour in the complex-time plane, see Fig. 14. Splitting the propagators and self-energies in statistical and spectral components yields the real and causal equations discussed in Sec. III. While for the NLO approximation this procedure is straightforward, it becomes cumbersome when multiloop contour integrals are encountered and integrals over products of sgn functions have to be evaluated. Here we give some general expressions we find useful.

First consider integrals over products of Θ -functions. Since the contribution from the upper and lower part of the contour differ only in sign, one finds e.g. that

$$\int_c dz^0 = 0, \quad \int_c dz^0 \Theta_c(x, z) = \int_0^{x^0} dz^0, \quad (\text{B1})$$

or in general

$$\int_c dz^0 \prod_{i=1}^M \Theta_c(x_i^0, z^0) = \sum_{i=1}^M \left[\prod_{j \neq i} \Theta_c(x_j^0, x_i^0) \right] \int_0^{x_i^0} dz^0. \quad (\text{B2})$$

Here we have taken the initial time at $z^0 = 0$. These results can be employed for integrals over products of sgn functions, using that $\text{sgn}_c(x, y) = 2\Theta_c(x, y) - 1$, yielding e.g.

$$\int_c dz^0 \text{sgn}_c(x, z) = 2 \int_0^{x^0} dz^0, \quad (\text{B3})$$

or in general

$$\int_c dz^0 \prod_{i=1}^M \text{sgn}_c(x_i^0, z^0) = 2 \sum_{i=1}^M \left[\prod_{j \neq i} \text{sgn}_c(x_j^0, x_i^0) \right] \int_0^{x_i^0} dz^0. \quad (\text{B4})$$

In a theory with quartic interactions, (B4) is needed with $M \leq 4$, for which we have verified this identity explicitly.

APPENDIX C: NUMERICAL SOLUTION OF THE SCHRÖDINGER EQUATION

In the case of quantum mechanics, we have the option to solve the Schrödinger equation numerically for the full wave function. This only applies to pure states, $\sigma = 1$. The system corresponds to a spherically symmetric anharmonic oscillator in N dimensions, and by imposing $O(N)$ symmetry and make suitable redefinitions we can reduce the problem to that of a particle on a half line in one dimension [15].

If the wave function is written as the product of a radial function, depending on the (rescaled) radial coordinate $0 < r = \sqrt{q_a q_a / N} < \infty$, and hyperspherical harmonics, depending on the $N - 1$ angles,

$$\Psi(q_a, t) = (Nr^2)^{(N-1)/4} \Phi(r, t) Y(\Omega), \quad (\text{C1})$$

the $O(N)$ symmetric problem is reduced to the effective one-dimensional Schrödinger equation [15]

$$\frac{i}{N} \frac{\partial}{\partial t} \Phi(r, t) = \mathcal{H}_{\text{eff}} \Phi(r, t), \quad (\text{C2})$$

with the Hamiltonian

$$\mathcal{H}_{\text{eff}} = -\frac{1}{2N^2} \frac{\partial^2}{\partial r^2} + U(r), \quad (\text{C3})$$

and the effective potential

$$U(r) = \frac{(1 - 1/N)(1 - 3/N)}{8r^2} + \frac{1}{2} m^2 r^2 + \frac{\lambda}{4!} r^4. \quad (\text{C4})$$

For a pure state the initial radial wave function, corresponding to the density matrix discussed in Sec. IV, is

$$\begin{aligned} \Phi(r, 0) &= \frac{1}{\sqrt{\frac{1}{2} \Gamma(N/2)}} \left(\frac{N}{2\xi^2} \right)^{N/4} r^{(N-1)/2} \\ &\times \exp \left[-N \left(\frac{1}{4\xi^2} + i \frac{\eta}{2\xi} \right) r^2 \right]. \end{aligned} \quad (\text{C5})$$

This initial wave function is normalized with respect to the inner product

$$\langle \Phi | \Phi \rangle = \int_0^\infty dr \Phi^\dagger(r, t) \Phi(r, t). \quad (\text{C6})$$

We solve Eq. (C2) numerically using the second-order Crank-Nicholson differencing scheme [30]. For the time intervals shown, both unitarity and energy are preserved better than 1 in 10^{12} .

[1] For a recent review, see J. Berges, AIP Conf. Proc. **739**, 3 (2004).

[2] Of course, perturbative or $1/N$ expansions in quantum mechanics and field theory are usually not convergent but

- instead asymptotic, see e.g. Ref. [31] for discussions concerning the $O(N)$ model.
- [3] For examples of nonequilibrium quantum field dynamics in the mean-field approximation, see e.g., F. Cooper, S. Habib, Y. Kluger, E. Mottola, J. P. Paz, and P. R. Anderson, Phys. Rev. D **50**, 2848 (1994); D. Boyanovsky, H. J. de Vega, R. Holman, D. S. Lee, and A. Singh, Phys. Rev. D **51**, 4419 (1995); D. Boyanovsky, H. J. de Vega, R. Holman, and J. F. Salgado, Phys. Rev. D **54**, 7570 (1996); D. Boyanovsky, C. Destri, H. J. de Vega, R. Holman, and J. Salgado, Phys. Rev. D **57**, 7388 (1998); J. Baacke, K. Heitmann, and C. Pätzold, Phys. Rev. D **58**, 125013 (1998), and references therein.
- [4] L. M. A. Bettencourt and C. Wetterich, Phys. Lett. B **430**, 140 (1998).
- [5] G. Aarts, G. F. Bonini, and C. Wetterich, Phys. Rev. D **63**, 025012 (2001).
- [6] Some scattering is present if one allows for inhomogeneous mean fields [32–34].
- [7] See e.g. Refs. [8,10,25,35] for the loop expansion, Refs. [16–18,20,22,36–38] for the 2PI-1/ N expansion to NLO, and Ref. [39] for 2PI dynamics with fermions.
- [8] A. Arrizabalaga, J. Smit, and A. Tranberg, Phys. Rev. D **72**, 025014 (2005).
- [9] E. Calzetta and B. L. Hu, Phys. Rev. D **37**, 2878 (1988).
- [10] S. Juchem, W. Cassing, and C. Greiner, Phys. Rev. D **69**, 025006 (2004); Nucl. Phys. A **743**, 92 (2004).
- [11] M. Lindner and M. M. Müller, Phys. Rev. D **73**, 125002 (2006).
- [12] J. Berges and S. Borsányi, hep-ph/0512155.
- [13] E. A. Calzetta, B. L. Hu, and S. A. Ramsey, Phys. Rev. D **61**, 125013 (2000).
- [14] G. Aarts and J. M. Martínez Resco, Phys. Rev. D **68**, 085009 (2003); J. High Energy Phys. 02 (2004) 061; 03 (2005) 074.
- [15] B. Mihaila, T. Athan, F. Cooper, J. Dawson, and S. Habib, Phys. Rev. D **62**, 125015 (2000); B. Mihaila, J. F. Dawson, F. Cooper, M. Brewster, and S. Habib, hep-ph/9808234.
- [16] G. Aarts and J. Berges, Phys. Rev. Lett. **88**, 041603 (2002).
- [17] K. Blagoev, F. Cooper, J. Dawson, and B. Mihaila, Phys. Rev. D **64**, 125003 (2001); F. Cooper, J. F. Dawson, and B. Mihaila, Phys. Rev. D **67**, 051901 (2003).
- [18] A. Arrizabalaga, J. Smit, and A. Tranberg, J. High Energy Phys. 10 (2004) 017.
- [19] In quantum field theory, stochastic quantization techniques have recently yielded the first real-time nonequilibrium lattice simulation results [40]. When developed further, this would offer the possibility for direct tests as well.
- [20] G. Aarts, D. Ahrensmeier, R. Baier, J. Berges, and J. Serreau, Phys. Rev. D **66**, 045008 (2002).
- [21] J. M. Cornwall, R. Jackiw, and E. Tomboulis, Phys. Rev. D **10**, 2428 (1974).
- [22] B. Mihaila, F. Cooper, and J. F. Dawson, Phys. Rev. D **63**, 096003 (2001).
- [23] S. R. Coleman, R. Jackiw, and H. D. Politzer, Phys. Rev. D **10**, 2491 (1974).
- [24] L. F. Abbott, J. S. Kang, and H. J. Schnitzer, Phys. Rev. D **13**, 2212 (1976).
- [25] G. Aarts and J. Berges, Phys. Rev. D **64**, 105010 (2001).
- [26] F. Cooper, S. Habib, Y. Kluger, and E. Mottola, Phys. Rev. D **55**, 6471 (1997).
- [27] In Ref. [15] only density matrices with $\eta = 0$ (and $\sigma = 1$) were considered.
- [28] This is different in field theory, where the amplitudes of equal-time correlation functions diminish in time due to dephasing. However, in the Hartree approximation the system still experiences recurrence. This shows that damping in the Gaussian approximation is not a result of irreversible loss of memory.
- [29] S. Jeon, Phys. Rev. D **52**, 3591 (1995); S. Jeon and L. G. Yaffe, Phys. Rev. D **53**, 5799 (1996).
- [30] W. H. Press, S. A. Teukolsky, W. T. Vetterling, and B. P. Flannery, *Numerical Recipes in C, Second Edition* (Cambridge University Press, United Kingdom, 1992).
- [31] J. Zinn-Justin, *Quantum Field Theory and Critical Phenomena* (Oxford University Press, New York, 1989); H. J. de Vega, Commun. Math. Phys. **70**, 29 (1979); J. Avan and H. J. de Vega, Phys. Rev. D **29**, 2904 (1984).
- [32] G. Aarts and J. Smit, Phys. Rev. D **61**, 025002 (2000).
- [33] M. Salle, J. Smit, and J. C. Vink, Phys. Rev. D **64**, 025016 (2001).
- [34] L. M. A. Bettencourt, K. Pao, and J. G. Sanderson, Phys. Rev. D **65**, 025015 (2002).
- [35] J. Berges and J. Cox, Phys. Lett. B **517**, 369 (2001).
- [36] J. Berges, Nucl. Phys. A **699**, 847 (2002).
- [37] J. Berges and J. Serreau, Phys. Rev. Lett. **91**, 111601 (2003).
- [38] F. Cooper, J. F. Dawson, and B. Mihaila, Phys. Rev. D **67**, 056003 (2003).
- [39] J. Berges, S. Borsányi, and J. Serreau, Nucl. Phys. B **660**, 51 (2003); J. Berges, S. Borsányi, and C. Wetterich, Phys. Rev. Lett. **93**, 142002 (2004).
- [40] J. Berges and I. O. Stamatescu, Phys. Rev. Lett. **95**, 202003 (2005).